Inorg. Chem. **2008**, *47*, 333–343

Proton-Coupled Electron Transfer in Ruthenium(II)–Pterin Complexes: Formation of Ruthenium-Coordinated Pterin Radicals and Their Electronic Structures

Soushi Miyazaki,[†] Takahiko Kojima,*[,†] Taisuke Sakamoto,[‡] Tetsuya Matsumoto,[‡] Kei Ohkubo,[†] and Shunichi Fukuzumi*[,†]

Department of Material and Life Science, Graduate School of Engineering, Osaka University and SORST (JST), Suita, Osaka 565-0871 and Department of Chemistry, Faculty of Sciences, Kyushu University, 6-10-1 Hakozaki, Higashi-Ku, Fukuoka 812-8581, Japan

Received September 7, 2007

Ruthenium(II)–pterin complexes were prepared using tetradentate and tripodal tris(2-pyridylmethyl)amine (TPA) and tris(5-methyl-2-pyridylmethyl)amine (5-Me_3-TPA) as auxiliary ligands together with 2-(*N*,*N*-dimethyl)-6,7-dimethylpterin (Hdmdmp) and 6,7-dimethylpterin (Hdmp) as pterin derivatives for ligands. Characterization was made by spectroscopic methods, X-ray crystallography, and electrochemical measurements. The pterin ligands coordinated to the ruthenium centers as monoanionic bidentate ligands via the 4-oxygen of the pyrimidinone moiety and the 5-nitrogen of the pyrazine parts. The striking feature is that the coordinated dmp^- ligand exhibits a quinonoid structure rather than a deprotonated biopterin structure, showing a short C–N bond length for the 2-amino group. Those complexes exhibit reversible two-step protonation for both pterin derivatives coordinated to the ruthenium centers to give a drastic spectral change in the UV–vis spectroscopy. Doubly protonated Ru(II)–pterin complexes were stabilized by π-back-bonding interaction and exhibited clear and reversible proton-coupled electron transfer (PCET) to give ruthenium-coordinated neutral monohydropterin radicals as intermediates of PCET processes. Those ESR spectra indicate that the unpaired electron delocalizes onto the PCET region (N5–C6–C7–N8) of the pyrazine moiety.

Introduction

Pterins are ubiquitous and redox-active fused heteroaromatic coenzymes, and they originated from guanosine.[1] It has been reported that GTP (guanosine triphosphate) is manipulated by a zinc enzyme of GTP cyclohydrolase I at the initial step of the folate biosynthesis in plants to be converted to dihydropterin triphosphate as an intermediate.[2] Physiological aspects of pterins have been investigated in terms of their relations to several diseases, including hematological neoplasias,[3] sudden infant death syndrome,[4] etc.

Pterin-dependent enzymes usually require cooperation of metal ions to conduct the enzymatic activity. This aspect differentiates them from flavin-containing enzymes, which are devoid of heavy metal requirements. Especially, all molybdenum enzymes except nitrogenase require pterins as cofactors in the vicinity of the metal centers.[5] Non-heme iron enzymes of phenylalanine hydroxylases are also pterin-dependent enzymes to hydroxylate the aromatic C−H bond to convert phenylalanine to tyrosine.[6] Heme enzymes such as nitric oxide synthases (NOS), which produce nitric oxide (NO) as an important neurotransmitter by oxidation of L-arginine with O_2, also contain pterins as cofactors in the vicinity of heme moieties.[7]

* To whom correspondence should be addressed. E-mail: kojima@chem.eng.osaka-u.ac.jp (T.K.) and fukuzumi@chem.eng.osaka-u.ac.jp (S.F.).
† Osaka University and SORST (JST).
‡ Kyushu University.

(1) Thöny, B.; Auerbach, G.; Blau, N. *Biochem. J.* **2000**, *347*, 1−16.
(2) Basset, G.; Quinlivan, E. P.; Ziemak, M. J.; Díaz de la Garza, R.; Fisher, M.; Schiffmann, S.; Bacher, A.; Gregory, J. F., III; Hanson, A. D. *Proc. Natl. Acad. Sci. U.S.A.* **2002**, *99*, 12489−12494.
(3) Denz, H. A.; Grünewald, K.; Thaler, J.; Huber, H.; Fuchs, D.; Hausen, A.; Reibnegger, G.; Werner, E. R.; Wachter, H. *Pteridines* **1989**, *1*, 167−170.
(4) Ambach, E.; Tributsch, W. *Pteridines* **1990**, *2*, 47−49.
(5) Hille, R. *Chem. Rev.* **1996**, *96*, 2757−2816.
(6) (a) Anderson, O. A.; Flatmark, T.; Hough, E. *J. Mol. Biol.* **2002**, *320*, 1095−1108. (b) Anderson, O. A.; Flatmark. T.; Hough, E. *J. Mol. Biol.* **2001**, *314*, 279−291. (c) Erlandsen, H.; Bjørgo, E.; Flatmark, T.; Stevens, R. C. *Biochemistry* **2000**, *39*, 2208−2217. (d) Kappock, T. J.; Caradonna, J. P. *Chem. Rev.* **1996**, *96*, 2659−2756.

10.1021/ic701759c CCC: $40.75
Published on Web 11/30/2007

Scheme 1. Summary of PCET Process of Pterins[a]

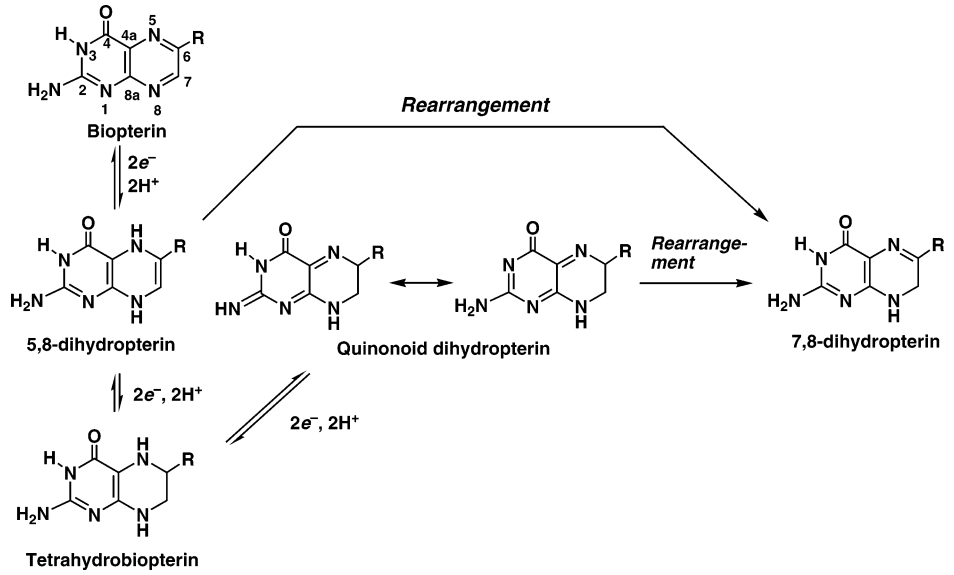

[a] The general numbering scheme for pterins is shown for the fully oxidized form (biopterin).

As for the molybdopterin enzymes, they have common structural features around the metal center including dithiolate ligands, exhibiting a variety of reactivity from oxidation to reduction.[8] It is generally assumed that such a variety of reactivity of those enzymes stems from the regulation of the redox potentials of pterin cofactors by virtue of noncovalent interactions between pterins and functional groups of protein backbones.[9] The noncovalent interactions include multiple hydrogen bonding toward pterin cofactors at the active sites and $\pi-\pi$ interactions in the vicinity of the metal centers. The 2-amino group is the part of the pterin structure involved in the majority of the hydrogen bonding interactions that include other electron-transfer groups such as iron−sulfur clusters as observed in aldehyde oxidoreductase[10] and reaction centers such as a heme moiety as found in inducible NOS.[11]

The fully oxidized form (biopterin) can accept up to 4-electrons/4-protons via proton-coupled electron transfer (PCET) to give the fully reduced form (tetrahydrobiopterin, H_4B) as shown in Scheme 1. The initial product of biopterin reduction is the 2-electron/2-proton product 5,8-dihydropterin, which is too unstable to be detected and spontaneously converts to the 7,8-dihydropterin.[12] The other dihydropterins such as the 2-electron/2-proton product of H_4B oxidation exhibits tautomerization between two kinds of so-called *quinonoid dihydropterin*, which includes a C−N double bond at the 2-amino group.[12b]

Several radical intermediates in the PCET process have been detected to elucidate the characteristics of the pterins both in vivo[13] and in vitro.[14] However, the poor resolution of ESR spectra of pterin-derived radicals in vivo has precluded clarifying their electronic structures.[13] In contrast, metal-free pterin cation radicals are formed under acidic conditions upon oxidation of 5,6,7,8-tetrahydropterin[15] and 6,6,7,7-tetramethyl-5,8-dihydropterin,[16] and they have been detected as well-resolved ESR spectra, which clearly demonstrate that the unpaired electron mainly localizes at the N-5 position.[5]

The collaboration of pterin cofactors with metal ions in the active sites of the metalloenzymes has encouraged coordination chemists to synthesize pterin−metal complexes to gain insight into the functionality of the cofactors in the enzymatic activity.[16,17] The redox behavior of metal-coordinated pterins has been investigated to understand the PCET process in the coordination spheres.[18] However, no report has been available on the detection of radical intermediates

(7) (a) Raman, C. S.; Li, H.; Martásek, P.; Král, V.; Masters, B. S. S.; Poulos, T. L. *Cell* **1998**, *95*, 939−950. (b) Crane, B. R.; Arval, A. S.; Ghosh, D. K.; Wu, C.; Getzoff, E. D.; Stuehr, D. J.; Tainer, J. A. *Science* **1998**, *279*, 2121−2126. (c) Aoyagi, M.; Arval, A. S.; Ghosh, D. K.; Stuehr, D. J.; Tainer, J. A.; Getzoff, E. D. *Biochemistry* **2001**, *40*, 12826−12832.

(8) CO dehydrogenase: Dobbek, H.; Gremer, L.; Kiefersauer, R.; Huber, R.; Meyer, O. *Proc. Natl. Acad. Sci. U.S.A.* **2002**, *99*, 15971−15976. DMSO reductase: (a) Schindelin, H.; Kisker, C.; Hilton, J.; Rajagopalan, K. V.; Rees, D. C. *Science* **1996**, *272*, 1615−1621. (b) George, G. N.; Doonan, C. J.; Rothery, R. A.; Boroumand, N.; Weiner, J. H. *Inorg. Chem.* **2007**, *46*, 2−4. Xanthine oxidoreductase: Okamoto, K.; Matsumoto, K.; Hille, R.; Eger, B. T.; Pai, E. F.; Nishino, T. *Proc. Natl. Acad. Sci. U.S.A.* **2004**, *101*, 7931−7936. See also: Burgmayer, S. J. N. *Prog. Inorg. Chem.* **2004**, *52*, 491−537.

(9) Wei, C.-C.; Crane, B. R.; Stuehr, D. J. *Chem. Rev.* **2003**, *103*, 2365−2383.

(10) Rebelo, J. M.; Dias, J. M.; Huber, R.; Moura, J. J. G.; Romão, M. J. *J. Biol. Inorg. Chem.* **2001**, *6*, 791−800.

(11) Crane, B. R.; Arvai, A. S.; Ghosh, S.; Getzoff, E. D.; Stuehr, D. J.; Tainer, J. A. *Biochemistry* **2000**, *39*, 4608−4621.

(12) (a) Burgmayer, S. J. N. *Struct. Bonding* **1998**, *92*, 67−119. (b) Benkovic, S. J.; Sammons, D.; Armarego, W. L. F.; Waring, P.; Inners, R. *J. Am. Chem. Soc.* **1985**, *107*, 3706−3712. (c) Raghavan, R.; Dryhurst, G. *J. Electroanal. Chem.* **1981**, *129*, 189−212. (d) Bobst, A. *Helv. Chim. Acta* **1967**, *50*, 2222−2225.

(13) For iNOS: Hurshman, A. R.; Krebs, C.; Edmondson, D. E.; Huynh, B. H.; Marletta, M. A. *Biochemistry* **1999**, *38*, 15689−15696. For aldehyde dehydrogenase (Mo−pterin): Luykx, D. M. A. M.; Dunie, J. A.; de Vries, S. *Biochemistry* **1998**, *37*, 11366−11375.

(14) Bobst, A. *Helv. Chim. Acta* **1968**, *51*, 607−613.

(15) Eberlein, G.; Bruice, T. C.; Lazarus, R. A.; Henrie, R.; Benkovic, S. J. *J. Am. Chem. Soc.* **1984**, *106*, 7916−7924.

(16) (a) Burgmayer, S. J. N. *Struct. Bonding* **1998**, *92*, 67−119. (b) Kaim, W.; Schwederski, B.; Heilmann, O.; Hornung, F. M. *Coord. Chem. Rev.* **1999**, *182*, 323−342.

by ESR spectroscopy to elucidate electronic structures of those radicals. This defect has hampered understanding the characteristics of metal-coordinated pterins and the influence of the metal ions on those electronic structures. In order to discuss the PCET of metal-bound pterins in connection with the uncoordinated counterparts, we need to have a *missing link* to describe a unified landscape of pterin chemistry.

We will present herein ruthenium(II)−pterin complexes showing PCET and the successful ESR detection of various radical intermediates to discuss the electronic characteristics of metal-coordinated pterins.[19] In this paper, we will focus on the significance of the 2-amino group of pterins in their properties including structural features and redox behavior in PCET. We used two pterin derivatives, *N*,*N*-dimethyl-6,7-dimethylpterin (Hdmdmp) and 6,7-dimethylpterin (Hdmp), to exemplify the impact of the 2-amino group on the redox behavior in terms of intermolecular hydrogen bonding. As ancillary ligands we employed tris(2-pyridylmethyl)amine (TPA) and tris(5-methyl-2-pyridylmethyl)amine (5-Me_3-TPA) to gain thermodynamic stability of the Ru(II)−pterin complexes by virtue of their electronic characteristics.[20]

Experimental Section

General. All chemicals available were purchased from appropriate commercial sources and used as received without further purification. $[RuCl(TPA)]_2(ClO_4)_2$,[20] $[RuCl(5\text{-}Me_3\text{-}TPA)]_2(ClO_4)_2$,[20] Hdmdmp,[21] Hdmp,[22] Na(dmp),[23] and 10,10′-dimethyl-9,9′,10,10′-tetrahydro-9,9′-biacridine $[(AcrH)_2]$[24] were prepared according to literature methods. All NMR measurements were performed on JEOL GX-400, EX-270, and AL-300 spectrometers. UV−vis absorption spectra were recorded on Jasco Ubest-50 UV/vis and Jasco V-570 spectrophotometers at room temperature unless otherwise noted. Infrared spectra were recorded on a Jasco IR model 800 infrared spectrophotometer. FAB-MS spectra were measured on a JMS-SX/SX 102A tandem mass spectrometer. Elemental analysis data for all compounds were obtained at the Service Center of the Elemental Analysis of Organic Compounds, Department of Chemistry, Kyushu University.

Safety Note: Perchlorate salts of metal complexes with organic ligands are potentially explosive. They should be handled with great care in small quantities.

Synthesis of [Ru(dmdmp)(TPA)]ClO_4 (1). $[RuCl(TPA)]_2(ClO_4)_2$ (0.100 g, 0.095 mmol) and Hdmdmp (0.083 g, 0.38 mmol) were suspended in methanol under N_2, and triethylamine (NEt_3: 50 μL, 0.40 mmol) was added. The mixture was refluxed for 6 h under N_2 and cooled to room temperature. Red crystalline materials precipitated and were collected and washed with diethyl ether and then dried in vacuo. Yield: 0.101 g, 75%. Anal. Calcd for $C_{28}H_{30}N_9O_5ClRu\cdot 1.5H_2O$: C, 45.68; H, 4.52; N, 17.12. Found: C, 45.88; H, 4.45; N, 17.11. UV−vis (in CH_3CN, λ_{max} (nm) (ϵ (M^{-1} cm^{-1})): 460 (1.40×10^4), 408 (1.46×10^4). ^1H NMR (CD_3CN, δ): 2.72 (s, 7-CH_3, 3H), 3.02 (s, −N(CH_3)$_2$, 6H), 3.14 (s, 6-CH_3, 3H), 4.51 (s, CH_2, 2H), 4.94 and 5.17 (ABq, J_{AB} =16 Hz, CH_2, 4H), 6.94 (td, 7 and 2 Hz, py-H5(ax), 1H), 7.06 (t, 6 Hz, py-H5(eq), 2H), 7.14 (d, 7 Hz, py-H3(ax), 1H), 7.31 (d, 8 Hz, py-H3(eq), 2H), 7.41 (td, 8 and 1 Hz, py-H4(ax), 1H), 7.62 (td, 8 and 2 Hz, py-H4(eq), 2H), 8.08 (dd, 5 and 2 Hz, py-H6(eq), 2H), 8.88 (d, 5 Hz, py-H6(ax), 1H).

Synthesis of [Ru(dmdmp)(5-Me_3-TPA)]ClO_4 (2). $[RuCl(5\text{-}Me_3\text{-}TPA)]_2(ClO_4)_2$ (0.300 g, 0.285 mmol) and Hdmdmp (0.250 g, 1.14 mmol) were suspended in MeOH (10 mL) under N_2, and NEt_3 (0.16 mL, 1.1 mmol) was added. The mixture was refluxed overnight under N_2 and cooled to room temperature. Purple crystalline materials precipitated and were collected and washed with diethyl ether and then dried in vacuo. Yield: 0.297 g, 69%. Anal. Calcd for $C_{31}H_{36}N_9O_5ClRu\cdot H_2O$: C, 48.40; H, 4.98; N, 16.39. Found: C, 48.57; H, 5.40; N, 16.27. ^1H NMR (CD_3CN, δ): 2.09 (s, 3H, 5-CH_3(ax) of 5-Me_3-TPA), 2.73 (s, 3H, 7-CH_3), 3.03 (s, 3H, 6-CH_3), 3.16 (s, 6H, N(CH_3)$_2$), 4.46 (s, 2H, CH_2(ax)), 4.90 and 5.10 (ABq, J_{AB} = 16 Hz, 4H, CH_2(eq)), 7.00 (d, 8 Hz, 1H, pyr-H3(ax)), 7.20 (d, 2H, 8 Hz, pyr-H3(eq)), 7.21 (d, 1H, pyr-H4(ax)), 7.43 (dd, 8 and 1 Hz, pyr-H4(eq)), 7.94 (s, 2H, pyr-H6(eq)), 8.76 (s, 1H, pyr-H6(ax)).

Synthesis of [Ru(dmp)(TPA)]ClO_4 (3). $[RuCl(TPA)]_2(ClO_4)_2$ (0.050 g, 47 mmol) and Na(dmp) (0.030 g, 0.14 mmol) were suspended in MeOH (7 mL) under N_2. The mixture was refluxed overnight under N_2 and cooled to room temperature. Red crystalline materials fell off and were collected and washed with diethyl ether and then dried in vacuo. Yield: 0.047 g, 81%. Anal. Calcd for $C_{26}H_{26}N_9O_5ClRu\cdot 2H_2O$: C, 43.55; H, 4.22; N, 17.58. Found: C, 43.32; H, 3.94; N, 17.11. Absorption maxima (λ_{max}, nm): 391 and 456. ^1H NMR (CD_3CN, δ): 2.73 (s, 3H, 7-CH_3), 3.17 (s, 3H, 6-CH_3), 4.51 (s, 2H, CH_2(ax)), 4.92 and 5.18 (ABq, J_{AB} = 16 Hz, 4H, CH_2(eq)), 5.10 (br-s, 2H, NH_2), 6.94 (t, 6 Hz, 1H, pyr-H5-(ax)), 7.06 (t, 7 Hz, 2H, pyr-H5(eq)), 7.14 (d, 7 Hz, 1H, pyr-H3-(ax)), 7.31 (d, 8 Hz, 2H, pyr-H3(eq)), 7.41 (t, 8 Hz, 1H, pyr-H4(ax)), 7.62 (td, 8 and 2 Hz, 2H, pyr-H4(eq)), 8.08 (d, 6 Hz, 2H, pyr-H6-(eq)), 8.88 (d, 5 Hz, 1H, pyr-H6(ax)).

Synthesis of [Ru(dmp)(5-Me_3-TPA)]ClO_4 (4). A mixture including $[RuCl(5\text{-}Me_3\text{-}TPA)]_2(ClO_4)_2$ (0.300 g, 0.285 mmol) and Na(dmp) (0.243 g, 1.14 mmol) in MeOH (10 mL) was refluxed under N_2 overnight. After cooling, the solvent was removed under reduced pressure. The residue was dissolved into CH_3CN, and insoluble materials were filtered off. The filtrate was dried up by

(17) For Mo: (a) Fischer, B.; Strähle, J.; Viscontini, M. *Pteridines* **1992**, *3*, 91−93. (b) Fischer, B.; Schmalle, H.; Dubler, E.; Schäfer, A.; Viscontini, M. *Inorg. Chem.* **1995**, *34*, 5726−5734. (c) Fischer, B.; Schmalle, H. W.; Baumgartner, M. R.; Viscontini, M. *Helv. Chim. Acta* **1997**, *80*, 103−110. (d) Burgmayer, S. J. N.; Arkin, M. R.; Bostick, L.; Dempster, S.; Everett, K. M.; Layton, H. L.; Paul, K. E.; Rogge, C.; Rheingold, A. L. *J. Am. Chem. Soc.* **1995**, *117*, 5812−5823. (e) Kaufmann, H. L.; Liable-Sands, L.; Rheingold, A. L.; Burgmayer, S. J. N. *Inorg. Chem.* **1999**, *38*, 2592−2599. (f) Kaufmann, H. L.; Carroll, P. J.; Burgmayer, S. J. N. *Inorg. Chem.* **1999**, *38*, 2600−2606. (g) Burgmayer, S. J. N.; Kaufmann, H. L.; Fortunato, G.; Hug, P.; Fischer, B. *Inorg. Chem.* **1999**, *38*, 2607−2613. For Cu: (h) Kohzuma, T.; Masuda, H.; Yamauchi, O. *J. Am. Chem. Soc.* **1989**, *111*, 3431−3433. (i) Odani, A.; Masuda, H.; Inukai, K.; Yamauchi, O. *J. Am. Chem. Soc.* **1992**, *114*, 6294−6300. (j) Perkinson, J.; Brodie, S.; Yoon, K.; Mosny, K.; Carroll, P. J.; Morgan, T. V.; Burgmayer, S. J. N. *Inorg. Chem.* **1991**, *30*, 719−727. (k) Mitsumi, M.; Toyoda, J.; Nakasuji, K. *Inorg. Chem.* **1995**, *34*, 3367−3370. (l) Lee, D.-H.; Murthy, N. N.; Lin, Y.; Nasir, N. S.; Karlin, K. D. *Inorg. Chem.* **1997**, *36*, 6328−6334.

(18) Abelleira, A.; Galang, R. D.; Clarke, M. J. *Inorg. Chem.* **1990**, *29*, 633−639.

(19) Kojima, T.; Sakamoto, T.; Matsuda, Y.; Ohkubo, K.; Fukuzumi, S. *Angew. Chem., Int. Ed.* **2003**, *42*, 4951−4954.

(20) (a) Kojima, T.; Amano, T.; Ishii, Y.; Ohba, M.; Okaue, Y.; Matsuda, Y. *Inorg. Chem.* **1998**, *37*, 4076−4085. (b) Kojima, T.; Matsuo, H.; Matsuda, Y. *Inorg. Chim. Acta* **2000**, *300*−*302*, 661−667.

(21) Funahashi, Y. Private communications. See also: Yamauchi, O.; Odani, A.; Masuda, H.; Funahashi, Y. In *Bioinorganic Chemistry of Copper*; Karlin, K. D., Tyeklár, Z., Eds.; Chapman & Hall: New York, 1993; p 363.

(22) Waring, P.; Armarego, W. L. F. *Aust. J. Chem.* **1985**, *38*, 629−631.

(23) Armarego, W. L. F.; Schou, H. *J. Chem. Soc., Perkin 1* **1977**, 2529−2536.

(24) (a) Fukuzumi, S.; Kitano, T.; Ishikawa, M. *J. Am. Chem. Soc.* **1990**, *112*, 5631−5632. (b) Fukuzumi, S.; Tokuda, Y. *J. Phys. Chem.* **1992**, *96*, 8409−8413.

a rotatory evaporator, and CH_2Cl_2 was added to redissolve it. Hexane was added to the solution to obtain a deep red precipitate, which was washed with ether and then dried in vacuo. Yield: 0.222 g, 54%. Anal. Calcd for $C_{29}H_{32}N_9O_5ClRu\cdot CH_3CN\cdot CH_3OH\cdot 3H_2O$: C, 45.20; H, 5.36; N, 16.26. Found: C, 45.54; H, 5.33; N, 16.47. ^{1}H NMR (acetone-d_6, δ): 2.17 (s, 3H, pyr-5-CH_3 (ax)), 2.70 (s, 3H, 7-CH_3), 3.36 (s, 3H, 6-CH_3), 5.30 and 5.08 (ABq, J_{AB} = 16 Hz, 4H, CH_2 (eq)), 5.16 (br s, 2H, NH_2) 7.17 (d, 8 Hz, 1H, pyr-H3 (ax)), 7.29 (d, 8 Hz, 1H, pyr-H4 (ax)), 7.35 (d, 8 Hz, 2H, pyr-H3 (eq)), 7.48 (d, 8 Hz 2H, pyr-H4 (eq)), 8.13 (s, 2H, pyr-H6 (eq)), 9.06 (s, 1H, pyr-H6 (ax)). UV/vis in CH_3CN: λ_{max} (nm) (ϵ (M^{-1} cm^{-1})): 462 (2.64×10^4), 377 (1.88×10^4), 255 (5.48×10^4).

X-ray Crystallography on 1. A single crystal of **1** was obtained from recrystallization from its methanolic solution. The crystal was efflorescent mounted in a glass capillary. All measurements were performed on a Rigaku RAXIS-RAPID imaging plate diffractometer at −180 °C with graphite-monochromated Mo Kα radiation (λ = 0.71073 Å). The data were collected with the $\omega-2\theta$ scan to the maximum 2θ value of 55.0° and corrected for Lorentz-polarization effects.

The structure was solved by direct methods and expanded using Fourier techniques. All non-hydrogen atoms were refined anisotropically. Refinement was carried out with full-matrix least squares on F with scattering factors[25] and including anomalous dispersion effects.[26] All calculations were performed using the teXsan crystallographic software package.[27]

X-ray Crystallography on 3. A single crystal of **3** was obtained by recrystallization from methanol with vapor diffusion of diethyl ether. A block-shaped red crystal was mounted on a glass capillary with silicon grease. All measurements were performed on a Rigaku Mercury CCD diffractometer at −170 °C with graphite-monochromated Mo Kα radiation (λ = 0.71070 Å) up to $2\theta_{max}$ = 55.0°.

The structure was solved by direct methods and expanded using Fourier techniques. All non-hydrogen atoms were refined anisotropically except two disordered ClO_4^- having 0.5 population for each. Refinement was carried out with full-matrix least squares on F with scattering factors from ref 23 and including anomalous dispersion effects. All calculations were performed using the Crystal Structure crystallographic software package,[28] and structure refinements were made using SHELX-97.[29]

Electrochemical Measurements. Cyclic voltammetry was employed in CH_3CN in the presence of 0.1 M [(n-butyl)$_4$N]PF_6 ($TBAPF_6$) as an electrolyte under N_2 at room temperature with use of a glassy carbon electrode as a working electrode, $Ag/AgNO_3$ as a reference electrode, and Pt wire as an auxiliary electrode. All potentials were calibrated with respect to the ferrocene/ferricenium redox couple as 0 V.

Controlled-potential electrolysis was carried out in a three-electrode cell using a BAS CV-27 voltammetry controller, modified for ESR and electronic absorption measurements. The working electrode was a Pt net of 0.3 mmϕ (1×1 cm^2). The auxiliary and reference electrodes were the same as those adopted in CV measurements. The reference electrode was separated from the solution by a salt bridge of a saturated [(n-butyl)$_4$N]ClO_4 (TBAP) solution in CH_3CN.

Spectroscopic Titration in Aqueous Media. In order to determine pK_a values of the pterin complexes **1** and **3** we used Britton−Robinson buffer, which is a mixed solution of KH_2PO_4, H_3BO_3, and CH_3COOH (molar ratio = 1:1:1) as a medium, and the titration was made by adding 0.1 M NaOH aqueous solution (pH > 2) or 70% $HClO_4$ (pH < 2) whose concentration was calibrated by a pH vs −log[$HClO_4$] plot. We applied the same procedure as that reported by Clarke and co-workers.[18] Absorbance at an appropriate wavelength (430 nm for **1** and 436 nm for **3**) was monitored, and curve fitting was made for A vs $(A - A')/[H^+]$ plots, where A' is the absorbance of the fully deprotonated complex and A is that at a given pH. This is based on the equation $pK_a = pH + \log\{(A - A')/(A^\circ - A)\}$. The plot affords $-K_a$ as the slope and A° as the intercept.

ESR Spectroscopy. ESR spectra were recorded on a JEOL JEX-REIXE spectrometer, and g values were determined using an Mn^{2+} marker. Controlled-potential electrolysis for ESR measurements was performed in CH_3CN using a HOKUTODENKO HSV-100 potentiostat in a handmade cell. As for the one-electron oxidation of **1** and **3**, a solution of **1** or **3** in CH_3CN (1 mM) was electrolyzed at 0.6 (for **1**) or 0.5 V (for **3**) (vs $Ag/AgNO_3$), respectively, in the presence of 0.1 M TBAP as an electrolyte. ESR spectra were measured in the range from −130 to −20 °C.

Concerning the one-electron reduction of a doubly protonated species of **1**, the electrolysis of 1.0 mM **1** in the presence of 5.0 mM $HClO_4$ and 0.1 M TBAP in CH_3CN was performed with an applied potential at −0.9 V (vs $Ag/AgNO_3$). In the case of the doubly protonated **3**, the one-electron reduction was made by photoirradiation (1000 W, high-pressure Hg lamp) of 1.0 mM of **3** in the presence of 5.0 mM $(AcrH)_2$ as an electron donor in C_2H_5CN at −70 °C.

Results and Discussion

Synthesis of the Complexes. Ru(II)−pterin complexes employed in this study were prepared in satisfactory yields using dimeric bis-μ-chloro complexes, $[RuCl(L)]_2^{2+}$ (L = TPA or 5-Me_3-TPA), as starting materials. Synthesis, however, using mononuclear [RuCl(L)(DMSO)]ClO_4 as a starting compound was unsuccessful. An outline of the synthesis is depicted in Scheme 2. Orange solutions of the dimer in MeOH turned deep red in the course of the reaction with pterins under basic conditions at reflux. The Ru(II)−pterin complexes are air stable and soluble in a wide range of solvents including water and CH_2Cl_2.

Concerning Ru(II)−dmdmp complexes, reaction of Hdmdmp in the presence of NEt_3 allowed us to obtain the target compounds in good yields. In contrast, reaction of Hdmp under the same conditions gave the products with contamination of impurity, from which we could not obtain pure Ru(II)−dmp complexes. Thus, we used the sodium salt of dmp^-, Na(dmp), as a starting material; then we could prepare pure Ru(II)−dmp complexes in good yields.

Molecular Structure of [Ru(dmdmp)(TPA)]$ClO_4\cdot 2H_2O$ ($1\cdot 2H_2O$). Recrystallization of the complex from methanol gave a red crystal suitable for X-ray crystallography. The crystal structure is shown in Figure 1 with numbering scheme. Selected bond lengths (Å) and angles (deg) are listed in Table 2 in comparison with those of **3** (vide infra). The

(25) Creagh, D. C.; McAuley, W. J. *International Tables for Crystallography*; Wilson, A. J. C., Ed.; Kluwer Academic Pulishers: Boston, 1992; Vol. C, Table 4.2.6.8, pp 219−222.
(26) Ibers, J. A.; Hamilton, W. C. *Acta Crystallogr.* **1964**, *17*, 781.
(27) *teXsan*: *Crystal Structure Analysis Package*; Molecular Structure Corp.: The Woodlands, TX, 1985 and 1999.
(28) *CrystalStructure 3.7.0*: *Crystal Structure Analysis Package*; Rigaku and Rigaku/MSC: The Woodlands, TX, 2000−2005.
(29) Sheldrick, G. M. *SIR 97 and SHELX 97, Programs for Crystal Structure Refinement*; University of Göttingen: Göttingen, Germany, 1997.

Scheme 2. Summary of Synthesis of Ruthenium(II)−Pterin Complexes

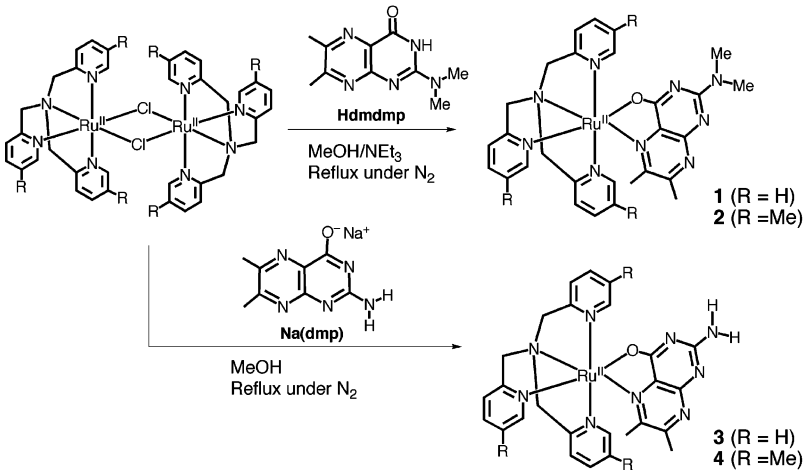

geometry around the ruthenium is a distorted octahedron with an angle of 164.4(3)° for N1−Ru1−N3, which is the meridional coordination part of TPA. The pterin ligand binds to the Ru^{II} center as a monoanion in a common fashion of O1−N5 chelating concomitant with a tetradentate TPA

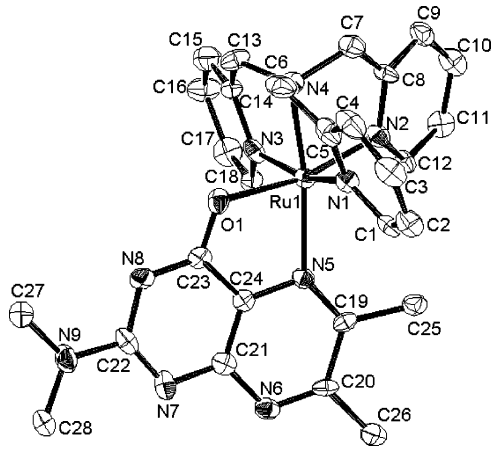

Figure 1. ORTEP drawing of the cation moiety of **1** with atomic numbering (50% probability thermal ellipsoids).

Table 1. X-ray Crystallographic Data for **1** and **3**

	1	**3**
formula	$C_{28}H_{36}N_9O_8ClRu$	$C_{26}H_{24}N_9O_7ClRu$
fw	763.17	711.05
cryst syst	monoclinic	triclinic
space group	$P2_1/c$ (No. 14)	$P\bar{1}$ (No. 2)
T, K	93	103
a, Å	17.768(4)	9.417(3)
b, Å	11.202(3)	10.993(4)
c, Å	17.723(5)	16.114(5)
α, deg	90	71.896(10)
β, deg	115.531(8)	84.248(11)
γ, deg	90	81.492(11)
V, Å^3	3183(1)	1565.4(9)
Z	4	2
no. of reflns measd	7928	11560
no. of observations	5070	6742
no. of params refined	425	385
$R1^a$	0.085 ($I > 3.0\sigma(I)$)	0.087 ($I > 2.0\sigma(I)$)
Rw^b	0.143 ($I > 3.0\sigma(I)$)^c	0.262 (all data)^d
GOF	1.473	1.080

^{a} $R1 = \sum ||F_o| - |F_c||/\sum|F_o|$. ^{b} $Rw = [\sum(w(F_o^2 - F_c^2)^2)/\sum w(F_o^2)^2]^{1/2}$. ^{c} $w = 1/(\sigma^2(F_o))$. ^{d} $w = 1/[\sigma^2(F_o^2) + (0.1126P)^2 + 9.5888P]$, where $P = (\max(F_o^2, 0) + 2F_c^2)/3$.

Table 2. Selected Bond Lengths (Å) and Angles (deg) of **1** and **3**

	1	**3**
Ru1−O1	2.083(5)	2.083(4)
Ru1−N1	2.082(7)	2.069(6)
Ru1−N2	2.086(6)	2.068(5)
Ru1−N3	2.050(8)	2.048(5)
Ru1−N4	2.041(7)	2.047(5)
Ru1−N5	2.107(6)	2.079(5)
O1−C23	1.272(10)	1.265(9)
N8−C23	1.322(10)	1.327(8)
N9−C22	1.369(9)	1.309(9)
N7−C22	1.32(1)	1.355(9)
N8−C22	1.37(1)	1.351(10)
O1−Ru1−N5	80.3(2)	80.6 (2)
N1−Ru1−N4	81.2(3)	82.0(2)
N2−Ru1−N4	80.8(3)	81.3(2)
N3−Ru1−N4	83.4(3)	84.5(2)
N1−Ru1−N2	100.7(3)	103.7(2)
O1−Ru1−N2	166.1(3)	165.85(18)
N1−Ru1−N3	164.4(3)	164.9(2)
N4−Ru1−N5	169.4(2)	171.8(2)

Scheme 3. Tautomerization of Deprotonated Pterin Derivatives

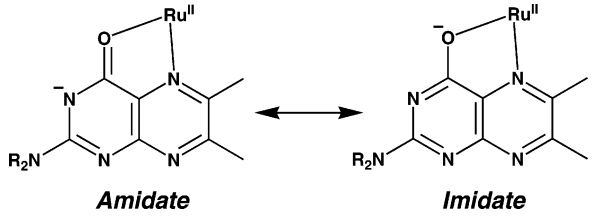

ligand. As for **1**, $dmdmp^-$ binds to the Ru^{II} center with bond lengths of 2.083(5) Å for Ru1−O1 and 2.107(6) Å for Ru1−N5 with a chelate angle of 80.3(2)°. Severe steric hindrance was observed between one methyl group of $dmdmp^-$ at the 6-position and one pyridine group including N2, defined as the axial pyridine, being reflected in the large N2−Ru−N5 angle of 100.9(3)° (Figure 1). This hindrance pushes away the pyrazine moiety of $dmdmp^-$ to result in a long bond distance of Ru1−N5 and tilts the pyridine ring from the pterin plane toward one equatorial pyridine moiety including N3 with a dihedral angle of 39.4(3)° between the pyrazine plane and the axial pyridine plane. Concerning the deprotonated amide moiety of $dmdmp^-$, two possible tautomers can be considered as shown in Scheme 3. In the case of **1**, the structure should be described as an *imidate* rather than an *amidate* based on the bond lengths of 1.272(10) Å for

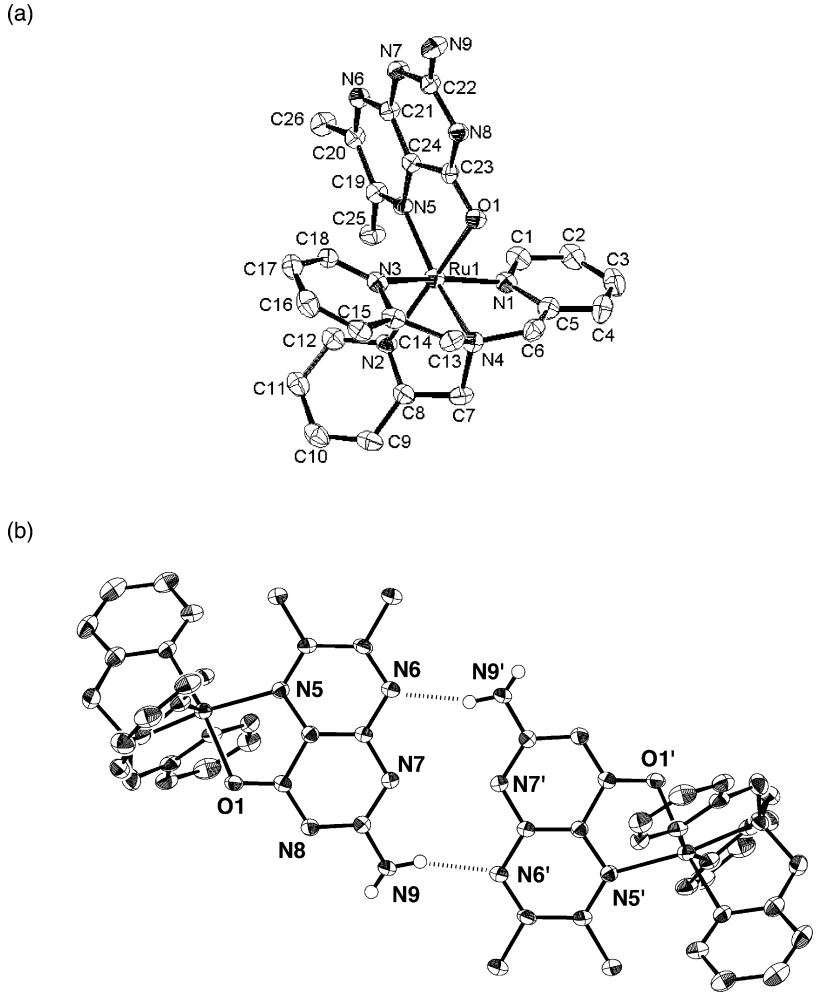

Figure 2. (a) ORTEP drawing of the cation moiety of **3** with 50% probability thermal ellipsoids with atomic-numbering scheme for non-hydrogen atoms. (b) Dimer formation of **3** in the crystal due to intermolecular hydrogen bonds.

O1−C23 and 1.322(10) Å for N8−C23. In addition, the imidate nitrogen (N8 in Figure 1) and the 1 position (N7 in Figure 1) form hydrogen bonding with water molecules of crystallization (N8···O8, 2.927(9) Å; N7···O6, 2.987 Å). The imidate coordination has been observed in $[M(NDMP^-)_2(MeOH)_2]$ (M = Fe, Co, Ni; $NDMP^-$ = deprotonated 2-dimethylamino-4(3*H*)-pteridinone)[30] and [Cu(tppb)(pterin)] (tbbp = tris(3-phenylpyrazolyl)hydroborate).[31] In contrast, Yamauchi and co-workers reported that Hdmdmp coordinates to a Cu^{II} center in $[Cu(NO_3)_2(Hdmdmp)_2]$[32] as a neutral ligand, and Burgmayer et al. also demonstrated that the amide is not deprotonated upon coordination in their Mo^{VI}−pterin complexes.[17e] This difference probably stems from that of interactions of pterins with metal d orbitals and the Lewis acidity of the Ru−TPA unit in which three pyridines act as π acceptors[33] to increase the acidity and facilitate deprotonation of Hdmdmp, leading to the imidate binding.

Molecular Structure of [Ru(dmp)(TPA)]ClO_4·2H_2O (3·2H_2O). Recrystallization of the complex from a methanol solution with vapor diffusion of diethyl ether gave a red crystal suitable for X-ray analysis. The crystal structure of the cation moiety of **3** is depicted in Figure 2a with numbering scheme. The geometry around the ruthenium center is octahedral with a more severe distortion at the axial pyridine coordination than in the dmdmp complex **1**. As for dmp^- coordination in **3**, the bond lengths of a Ru1−O1 and Ru1−N5 are determined as 2.083(4) and 2.079(5) Å, respectively, and the chelate angle is 80.6 (2)° for O1−Ru1−N5. The dihedral angle between the mean plane of the dmp ligand and that of the axial pyridine ring is estimated to be 48.0°, which is larger than that in **1** as mentioned above. This would be caused by the shorter bond length of Ru1−N5 (2.079(5) Å) in **3** than that (2.107(6) Å) in **1**. This shorter bond pushes the 6-methyl group toward the axial pyridine of TPA to cause the severe tilt.

(30) Funahashi, Y.; Hara, Y.; Masuda, H.; Yamauchi, O. *Inorg. Chem.* **1997**, *36*, 3869−3875.

(31) Perkinson, J.; Brodie, S.; Yoon, K.; Mosny, K.; Carroll, P. J.; Morgan, T. V.; Burgmayer, S. J. N. *Inorg. Chem.* **1991**, *30*, 719−727.

(32) Yamauchi, O.; Odani, A.; Masuda, H.; Funahashi, Y. In *Bioinorganic Chemistry of Copper*; Karlin, K. D., Tyeklár, Z., Eds.; Chapman & Hall: New York, 1993; p 363. Regarding the coordination of pterins to Cu(II) ion, pterins like Hdmp coordinate to Cu(II) centers both with and without deprotonation of the N-3 position, which depends on the Cu(II) salts used and addition of a base: Kohzuma, T.; Odani, A.; Morita, Y.; Takani, M.; Yamauchi, O. *Inorg. Chem.* **1988**, *27*, 3854−3858.

(33) (a) Kojima, T; Matsuda, Y. *J. Chem. Soc., Dalton Trans.* **2001**, 958−960. (b) See also ref 20a.

Scheme 4. Resonance Structures of Coordinated Pterins

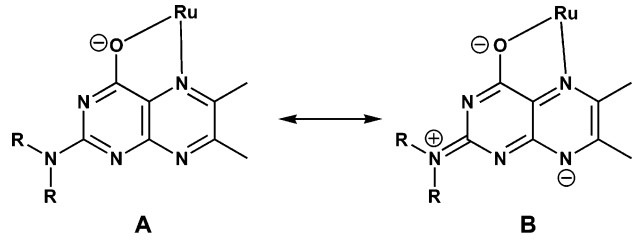

A remarkable difference can be found in the bond length of the 2-amino group: the N9−C22 distance in **3** is 1.309(2) Å, which is extremely short for a C−N single bond and rather close to a C═N double bond as found in a quinonoid derivative (1.293(5) Å).[34] The bond length is also much shorter than that (1.369(9) Å) observed in **1**. According to a database,[35] the average of planar C(aromatic)−N(sp^2)H_2 bond lengths is 1.355(20) Å and that of planar C(aromatic)−N(sp^2)(C_n)$_2$ is 1.371(16) Å; thus, little difference is observed. Therefore, the bond length of the C−N bond for the 2-amino group in the dmp$^-$ ligand seems to be influenced by intermolecular hydrogen bonding of the amino group with outer entities, such as a water molecule of crystallization and another molecule. Actually, in the crystal of **3**, intermolecular hydrogen bonds are found between the 2-amino group (N9) and the nitrogen at the 8 position (N6) of the dmp$^-$ ligands with a distance of 2.905 Å with 161.3° for −N6−H26−N9 as shown in Figure 2b. In addition, the amino group (N9) also forms a hydrogen bond with a water molecule of crystallization, exhibiting 2.842 Å separation with 154.9° for O10−H25−N9. The water molecule of crystallization also forms another hydrogen bond with the 3 position of an adjacent molecule (N8) to afford a hydrogen-bonding network in the crystal (see Supporting Information). The interatomic distance between N7···N7′ is 2.839 Å, and this short separation can cause electrostatic repulsion between the lone pairs of the nitrogen atoms, whereas the intermolecular hydrogen bonding is preferred for the pterin molecules. Several patterns of intermolecular hydrogen bonding have been reported for other pterin−metal complexes. However, it should be emphasized that this type of dimerization by intermolecular hydrogen bonding in Figure 2 is unprecedented.

Dimer formation between the amino group and the 8-position by the hydrogen bonding suggests that the most basic site of the pterin is the 8-position, which should be protonated first as demonstrated by ESR measurements (vide infra) rather than the deprotonated 3-position in the imidate moiety. Such a short C−N bond has been observed in the crystal structure of a Mo(IV) complex bearing tetrahydropterin in which the bond distance has been reported to be 1.308(4) Å and the 2-amino group undergoes two hydrogen bonds.[36] In the case of single hydrogen bonding of the 2-amino group, the C−N bond length is longer than that in the case of the doubly hydrogen-bonded one.[37] This suggests that the stabilization of the quinonoid form depicted in Scheme 4 is gained by two hydrogen bonds involving the 2-amino group. Viscontini and co-workers also noted formation of quinonoid structures in Mo coordination spheres based on the short bond distances.[17a−c]

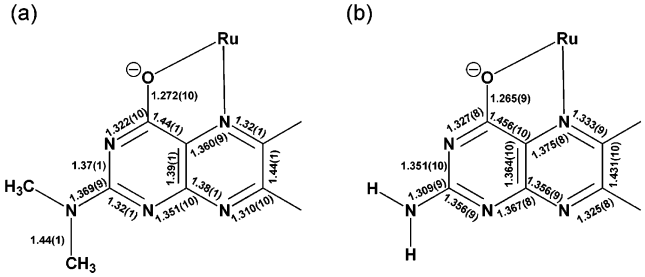

Figure 3. Bond lengths (Å) of pterin ligands in **1** (a) and **3** (b).

The bond lengths of N7−C22 in the pyrimidinone rings also showed a difference, 1.32(1) Å for **1** and 1.356(9) Å for **3**. This should be caused by intermolecular hydrogen bonds toward the 2-amino group of the dmp ligand. The intermolecular hydrogen bonds make the amino nitrogen more negative due to the polarization of the N−H bonds of the amino group, which cannot be induced in the case of the *N*,*N*-dimethyl group as in the dmdmp ligand. This results in the stabilization of a resonance structure of B (a quinonoid form) over A in Scheme 4 and gives a double-bond character for the amino group. Along this line, the N7−C22 bond bears a single-bond character in **3** and, in contrast, a double-bond character in **1**. As reflected in those bond lengths (Figure 3), resonance structures can be depicted in Scheme 4. For complex **1**, structure A is dominant, whereas structure B is dominant for complex **3**.

Spectroscopic Characterization of Ruthenium(II)−Pterin Complexes. NMR spectra of **1**−**4** exhibited a typical σ_h pattern for the TPA and 5-Me_3-TPA ligands.[20] The methylene hydrogen atoms of the TPA ligands showed one singlet for the axially bound pyridylmethyl moiety and one AB quartet for the two equatorial pyridylmethyl arms. This indicates that the axial pyridine rings can move across the symmetric plane in solutions, whereas the crystal structures exhibit their severe tilts due to the steric hindrance with the 6-methyl groups of the dmdmp$^-$ and dmp$^-$ ligands.

In the ^{1}H NMR spectrum of **1** in CD_3CN, a signal assigned to the methyl groups on the amino nitrogen gave one singlet at 3.02 ppm even though they should be nonequivalent, and those for the 6-methyl and the 7-methyl groups were observed at 3.14 and 2.72 ppm as singlets, respectively.

Concerning that of **3**, singlets due to the 6- and 7-methyl groups were observed at 3.17 and 2.73 ppm, respectively. In addition, a broad singlet ascribed to the amino protons was detected at 5.12 ppm, which diminished upon addition of D_2O.

The ^{1}H NMR spectra of **2** and **4** showed similar spectral features as observed in **1** and **3**. Singlet peaks due to the 6-

(34) Noar, J. B.; Venkataram, U. V.; Bruice, T. C.; Bollag, G.; Whittle, R.; Sammons, D.; Henry, R.; Benkovic, S. J. *Bioorg. Chem.* **1986**, *14*, 17−27.

(35) *CRC Handbook*, 82nd ed.; CRC Press: Boca Raton, FL, 2001; pp 9−6. An average of imine C═N bond lengths is 1.279(8) Å.

(36) Fisher, B.; Schmalle, H. W.; Baumgartner, M. R.; Viscontini, M. *Helv. Chim. Acta* **1997**, *80*, 103−110.

(37) Bieri, J. H. *Helv. Chim. Acta* **1977**, *60*, 2303−2308.

and 7-methyl groups were detected at 3.03 and 2.73 ppm for **2** and 3.36 and 2.70 ppm for **4**, respectively. In addition, a broad singlet assigned to the NH_2 of the 2-amino group was observed at 5.16 ppm for **2**, which overlapped with one of the AB quartets derived from the methylene protons and also diminished upon adding D_2O. Thus, the 5-Me_3-TPA derivatives of pterin complexes **2** and **4** should have the same structures as those of **1** and **3**.

Absorption Spectroscopy: Reversible Protonation−Deprotonation. The absorption spectrum of **1** in CH_3CN exhibits absorption maxima at 459 and 407 nm due to MLCT bands from dπ orbitals of Ru(II) ion to π* orbitals of the dmdmp$^-$ ligand. These absorption bands are shifted to 456 and 391 nm for **3**, respectively. This is due to a stronger interaction of the dmp$^-$ ligand with the Ru(II) center than that of the dmdmp$^-$ ligand as reflected in the shorter bond lengths as described above (Table 2). The stronger interaction causes a larger ligand field splitting at the Ru^{II} center, and this gives rise to the blue shift as observed.

A reversible protonation−deprotonation behavior is found in the UV−vis spectra of **1**−**4** (vide infra). Upon addition of $HClO_4$ (70% aq), the orange color of **1** turns to blue, accompanied by the appearance of a new absorption at 595 nm, which is assigned to a MLCT band due to transition from the Ru^{II} center to a doubly protonated pterin ligand and also absorption in the range of 330−430 nm due to a $\pi-\pi$* transition of coordinated H_2dmdmp$^+$. The original spectrum was recovered by adding NEt_3, indicating this protonation−deprotonation is reversible. This is due to the strong π-back-bonding to the pterin cation from the Ru^{II} center as indicated by the intense MLCT band for the protonated complex. The double protonation of the pterin ligands lowers the MLCT transition energy and the energy level of π* orbitals to facilitate the π-back-bonding from the filled dπ orbitals to the π* orbitals of the protonated pterin ligands.[38] In the case of **3**, double protonation gave a new intense absorption assignable to a MLCT from Ru(dπ) to pterin(pπ*) at 536 nm in CH_3CN, which is blue shifted from that in the case of **1**. This indicates that the energy level of the pπ* orbital of H_2dmp$^+$ is higher than that of H_2dmdmp$^+$. This blue shift of the MLCT band of the doubly protonated **3** is supported by the redox potentials of Ru^{II}/Ru^{III} redox couples for doubly protonated **1** (0.54 V) and **3** (0.57 V); as described in the following section, a lower dπ level for **3** than that of **1**; it is also consistent with the order of reduction potentials of the protonated pterin ligands, −0.64 V for [Ru(H_2dmp$^+$)(TPA)]$^{3+}$ and −0.66 V for [Ru(H_2dmdmp$^+$)(TPA)]$^{3+}$ (vide infra). Thus, the energy gap between the dπ orbital of Ru(II) and the pπ* of the doubly protonated pterins for [Ru(H_2dmp$^+$)(TPA)]$^{3+}$ is larger than that of [Ru(H_2dmdmp$^+$)(TPA)]$^{3+}$.

Scrutiny into the protonation process allowed us to reveal that two stepwise protonations occur to the pterin ligands. We measured the UV−vis spectra of **1** and **3** in Britton−Robinson buffer solutions at room temperature, and titrations

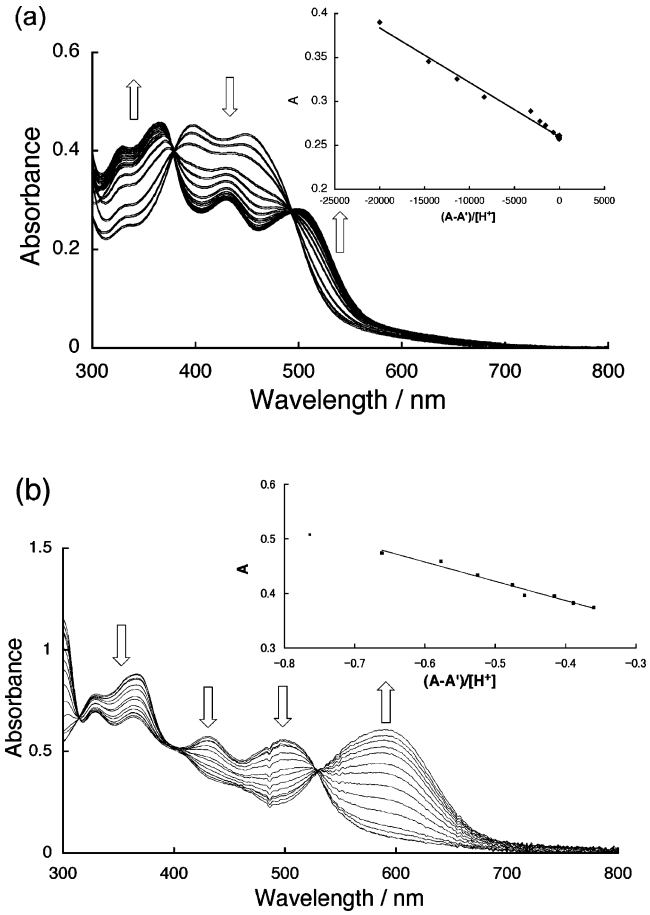

Figure 4. UV−vis spectral changes of **1** in aqueous Britton−Robinson buffer: (a) the first protonation step and (b) the second protonation step. (Insets) Plots of A versus $(A - A')/[H^+]$. A represents absorbance at 430 nm.

were performed by adding aqueous $HClO_4$ to observe spectral changes. The first protonation process of **1** to form [Ru(Hdmdmp)(TPA)]$^{2+}$ results in the spectral change to exhibit absorption maxima at 502, 429, 366, and 327 nm with two isosbestic points at 493 and 379 nm in Figure 4a. The second protonation to generate [Ru(H_2dmdmp$^+$)(TPA)]$^{3+}$ proceeds to give a blue solution exhibiting an absorption maximum at 592 nm as shown in Figure 4b. In this process three isosbestic points were observed at 314, 399, and 529 nm. In both cases, plots of A versus $(A - A')/[H^+]$ (insets of Figure 4a and b), where A' is the absorbance of the fully protonated complex and A is the absorbance of at a given pH, showed a linear relationship to allow us to determine the K_a value from the slope. On this basis we determined the pK_a values of the two-step protonation of **1** in an aqueous solution as pK_{a1} = 5.21 and pK_{a2} = 0.45. Similarly, pK_a values for **3** were determined to be pK_{a1} = 5.45 and pK_{a2} = 0.57 (see Supporting Information). The pK_a values of the pterin complexes are nearly the same regardless of the difference between the amino group and the *N*,*N*-dimethylamino group. The pK_a values are summarized in Table 3 together with redox potentials.

Electrochemical Measurements to Probe PCET. Cyclic voltammetry (CV) was performed in CH_3CN containing 0.1 M TBAP as an electrolyte at room temperature under N_2. Potentials were determined relative to that of the ferrocene/

(38) Shin, Y. K.; Brunschwig, B. S.; Creutz, C.; Newton, M. D.; Sutin, N. *J. Phys. Chem.* **1996**, *100*, 1104−1110 and references cited therein.

Table 3. Summary of Redox Potentials ($E_{1/2}$) and pK_a Values for **1** and **3** in CH_3CN[a]

	oxidation		reduction			
	Ru^{II}/Ru^{III}	$P^-/P^{2-\bullet}$	$P^{2-\bullet}/P^{3-}$	$H_2P^+/H_2P^\bullet$	pK_a1[b]	pK_a2[b]
$[Ru(dmdmp)(TPA)]^+$ (**1**)	0.26	−2.08	n.d.[c]		5.21	0.45
$[Ru(dmp)(TPA)]^+$ (**3**)	0.27	−2.04	irreversible		5.45	0.57
doubly protonated form[d]						
$[Ru(H_2dmdmp)(TPA)]^{3+}$	0.54			−0.66		
$[Ru(H_2dmp)(TPA)]^{3+}$	0.57			−0.64		

[a] Potentials were determined relative to a ferrocene/ferricenium redox couple as 0 V. All measurements were carried out in CH_3CN in the presence of 0.1 M $TBAPF_6$ as an electrolyte at room temperature under N_2. [b] The pK_a values were determined in aqueous Britton−Robinson buffer solutions. [c] Not detected. [d] Protonation was made by adding aqueous $HClO_4$ (70%) in 10-fold excess into the CH_3CN solutions.

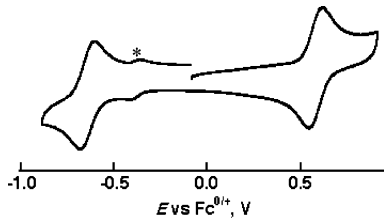

Figure 5. Cyclic voltammogram of $[Ru(H_2dmp^+)(TPA)]^{3+}$ in CH_3CN (0.1 M $TBAPF_6$) at room temperature: a mixture of 1 mM of **3** and 2 mM of $HClO_4$. A small redox wave with an asterisk has yet to be assigned.

ferricenium redox couple as 0 V. Complexes **1**−**4** exhibited two reversible and one quasi-reversible redox waves within the range from −2 to +1 V. The redox potentials are summarized in Table 3 for **1** and **3** with those doubly protonated forms.

The redox waves assigned to Ru^{II}/Ru^{III} redox couples were observed at 0.26 V ($\Delta E = E_{pa}(ox) - E_{pc}(red) = 61$ mV) for **1** and 0.27 V ($\Delta E = 67$ mV) for **3**, respectively. As for reduction of the pterin complexes, reductions of the pterin ligands were observed at −2.08 V ($\Delta E = 60$ mV) for **1** and −2.04 V ($\Delta E = 72$ mV) for **3**, attributable to formation of $dmdmp^{2-\bullet}$ and $dmp^{2-\bullet}$, respectively, in the ruthenium coordination sphere. Therefore, reduction occurs at nearly the same potential for both ligands without protonation.

On the other hand, upon addition of aqueous $HClO_4$, the redox couples for the Ru(II)−pterin complexes are shifted to higher potentials due to protonation as summarized in Table 3. The impact of the protonation to the redox potentials of the Ru^{II}/Ru^{III} redox couples is similar for **1** ($\Delta E_{1/2} = +0.28$ V) and **3** ($\Delta E_{1/2} = +0.30$ V), and the resultant potentials are nearly the same. This indicates that the HOMO (Ru d_π) levels are comparable as mentioned above.

The protonated form of **1** and that of **3** exhibited clear reversibility in the reduction of the protonated pterin ligands. As can be seen in Figure 5, the CV of doubly protonated **3** ($[Ru(H_2dmp^+)(TPA)]^{3+}$) showed a reversible redox wave at −0.64 V ($\Delta E = 76$ mV), which was assigned to the coordinated $H_2dmp^+/H_2dmp^\bullet$ redox couple by ESR measurements with bulk electrolysis as described below. In the case of the doubly protonated **1** ($[Ru(H_2dmdmp^+)(TPA)]^{3+}$), the first reduction observed at −0.66 V ($\Delta E = 90$ mV) is also fairly reversible to form the coordinated $H_2dmdmp^\bullet$. It is noteworthy that the relatively large positive shift (+1.4 V) of the one-electron reduction potentials of the doubly protonated complexes can be observed relative to the reduction potentials of the pterin ligands in **1** and **3**.

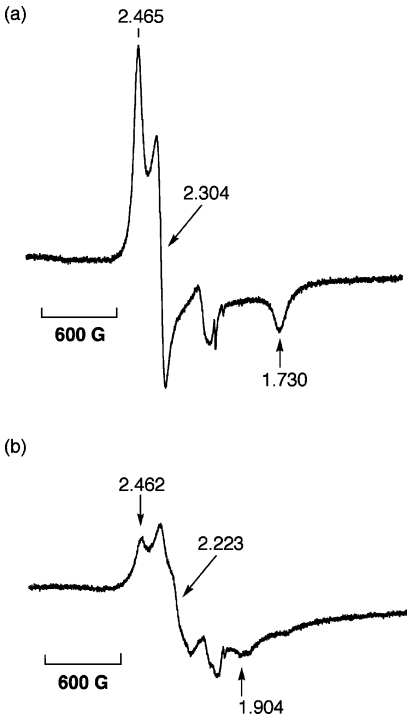

Figure 6. ESR spectra of one-electron-oxidized species of **1** (a) and **3** (b) (1.0×10^{-3} M) generated by electrolysis at an applied potential of 0.6 V (vs $Ag/AgNO_3$) in CH_3CN containing 0.1 M Bu_4NClO_4, measured in frozen CH_3CN at 173 K.

ESR Measurements. In order to confirm the assignments of the redox waves observed in CV measurements, we conducted bulk electrolysis to measure ESR spectra of oxidized or reduced species in CH_3CN containing 0.1 M TBAP as an electrolyte. These measurements allow us to gain insight into the electronic structures and characteristics of those species.

The electrochemical one-electron oxidation of **1** in CH_3CN at room temperature afforded the corresponding Ru(III) complex, $[Ru^{III}(dmdmp)(TPA)]^{2+}$, which exhibited a typical $S = 1/2$ signal with anisotropy as depicted in Figure 6a. The signal showed three g values of 2.465, 2.304, and 1.730. This result allowed us to assign the first oxidation to be the Ru^{II}/Ru^{III} process. The spectrum exhibited no temperature dependence in the range of 173−223 K, indicating no valence-tautomerization in the Ru^{III}−dmdmp complex. In the case of **3**, we could observe a similar spectrum assigned to the Ru(III) complex, $[Ru^{III}(dmp)(TPA)]^{2+}$, exhibiting anisotropic g values of 2.462, 2.223, and 1.904, as can be seen in Figure 6b. It is surprising that an ESR

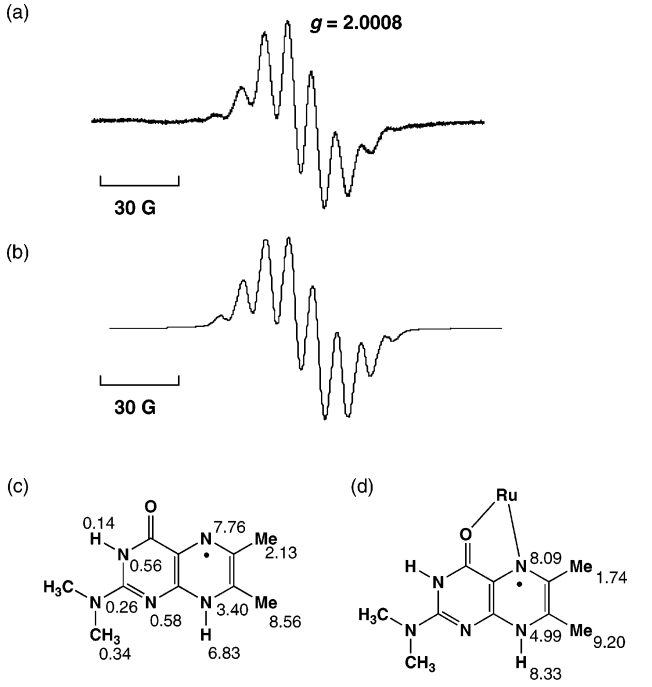

Figure 7. (a) ESR spectrum of $[Ru(H_2dmdmp^{\bullet})(TPA)]^{2+}$ generated by electrolysis at −0.9 V (vs $Ag/AgNO_3$) in CH_3CN (0.1 M TBAP); measured at 253 K. (b) The computer simulation spectrum with ΔH_{msl} (maximum slope line width) = 1.8 G. (c) Hyperfine coupling constants based on spin density obtained by DFT calculations. (d) The hyperfine coupling constants used for the simulation. Values are given in gauss.

signal due to a Ru(III) complex can be observed at such higher temperatures since no signals have been observed for mononuclear Ru(III) complexes such as $[RuCl_2$(TPA derivative)$]^+$ even at 4 K.[39] We also observed an ESR signal derived from a Ru(III) complex having deprotonated alloxazine, which is a flavin analogue.[40] However, the reason why the ESR signal can be detected at such high temperatures for those Ru(III) complexes with coenzymes as ligands has yet to be clarified.

The second protonation process enables one to obtain positively charged pterin ligands, $[Ru(H_2dmdmp)(TPA)]^{3+}$ and $[Ru(H_2dmp)(TPA)]^{3+}$ (vide supra). The stability of the coordination of protonated and positively charged pterin ligands should be derived from the π-back-donation from the ruthenium center to the lowered pπ* orbitals of the protonated pterin ligands. The doubly protonated complexes could be reduced by controlled-potential bulk electrolysis to give ruthenium-substituted monohydropterin radicals as intermediates of their PCET. The one-electron reduced species of $[Ru(H_2dmdmp^+)(TPA)]^{3+}$, i.e., $[Ru(H_2dmdmp\bullet)(TPA)]^{2+}$, was generated in CH_3CN (0.1 M TBAP) at −20 °C by electrolysis at −0.9 V (vs $Ag/AgNO_3$) to measure its ESR spectrum.

The ESR spectrum of electrochemically generated $[Ru(H_2dmdmp^{\bullet})(TPA)]^{2+}$ in CH_3CN is shown in Figure 7a.[19] The observed spectrum is well reproduced by the computer simulation spectrum in Figure 7b, which afforded the hyperfine coupling (*hfc*) constants. The DFT calculations at the UB3LYP/6-31G(d) level of theory without the ruthenium ion (Figure 7c) suggested assignment of the *hfc* value at each nucleus as shown in Figure 7d.[41] The important point indicated by the ESR spectrum is that the unpaired electron is delocalized only on the N5−C6−C7−N8 region where the PCET occurs.

Scheme 5. Photoinduced Electron Transfer to Generate the Ru(II)-Bound $H_2dmp\bullet$ in C_2H_5CN at −70 °C

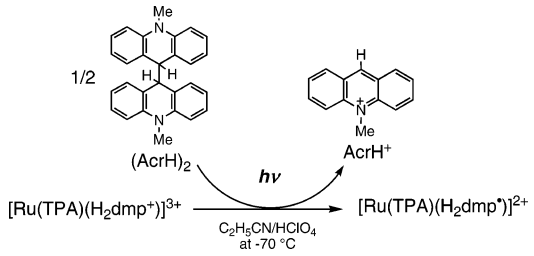

In order to generate the one-electron reduced species of $[Ru(H_2dmp^+)(TPA)]^{3+}$ ($[Ru(H_2dmp^{\bullet})(TPA)]^{2+}$) we applied a photoinduced electron-transfer (PET) reaction with 10,10′-dimethyl-9,9′-biacridine ($(AcrH)_2$) used as a reducing reagent as depicted in Scheme 5.[42] A solution of $[Ru(H_2dmp^+)(TPA)]^{3+}$ and $(AcrH)_2$ in C_2H_5CN at −70 °C was illuminated with a high-pressure Hg lamp (1000 W). The PET reaction successfully generated the radical-coordinated complex to allow us to observe its well-resolved ESR signal. The ESR spectrum of $[Ru(H_2dmp^{\bullet})(TPA)]^{2+}$ is shown in Figure 8a with its simulation spectrum (Figure 8b). The predicted *hfc* values by DFT calculations (Figure 8c) allow us to assign the observed *hfc* values for this ruthenium-bound monohydropterin radical as shown in Figure 8d. This result clearly indicates that the unpaired electron is also delocalized on the PCET region as observed in the $H_2dmdmp^{\bullet}$ complex. The *hfc* values for this species are slightly different from those of the dmdmp counterpart; however, the electronic structures are virtually the same for both pterin radicals.

The DFT calculations at the UB3LYP/6-31G(d) level of theory on those radicals allowed us to visualize the distribution of spin density in $H_2dmp^{\bullet}$ and $Hdmdmp^{\bullet}$ as shown in Figure 9. The spin density obviously delocalizes in π* orbitals of pterins over the pyrazine moiety rather than the pyrimidinone part in both cases. It has previously been reported that the spin densities of monohydropterin radicals are in the order N5 > C7 ≈ N8 > C6.[44] The trend is a little different in the radicals observed in our DFT calculations:

(39) Kojima, T.; Hayashi, K.; Matsuda, Y. Unpublished results. See also: Kojima, T.; Hayashi, K.; Iizuka, T.; Tani, F.; Naruta, Y.; Kawano, M.; Ohashi, Y.; Hirai, Y.; Ohkubo, K.; Matsuda, Y.; Fukuzumi, S. *Chem. Eur. J.* **2007**, *13*, 8212−8222.

(40) Miyazaki, S.; Ohkubo, K.; Kojima, T.; Fukuzumi, S. *Angew. Chem., Int. Ed.* **2007**, *46*, 905−908.

(41) We examined other basis data sets for the DFT calculations for estimating hyperfine coupling constants with nitrogen and hydrogen nuclear spins as listed in Tables S1 and S2 of Supporting Information. The results obtained exhibited similar tendency, and the most appropriate values were obtained by the UB3LYP/6-31G(d) level of theory.

(42) (a) Fukuzumi, S.; Koumitsu, S.; Hironaka, K.; Tanaka, T. *J. Am. Chem. Soc.* **1987**, *109*, 305−316. (b) Yuasa, J.; Yamada, S.; Fukuzumi, S. *Angew. Chem., Int. Ed.* **2007**, *46*, 3553−3555.

(43) $[Ru(H_2dmp^{\bullet})(TPA)]^{2+}$ was not stable enough to be detected by ESR under the electrolysis conditions.

(44) Ehrenberg, A.; Hemmerich, P.; Müller, F.; Pfleiderer, W. *Eur. J. Biochem.* **1970**, *16*, 584−591.

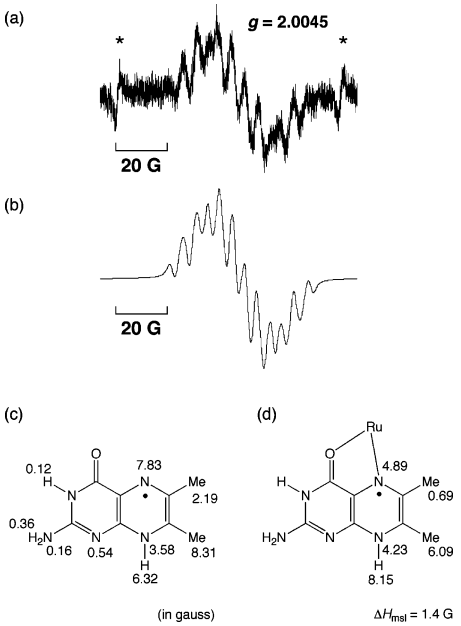

Figure 8. (a) ESR spectrum of $[Ru(H_2dmp^{\bullet})(TPA)]^{2+}$ produced by photoinduced electron transfer from $(AcrH)_2$ (5.0×10^{-4} M) to $[Ru(dmp)(TPA)]^{+}$ (1.0×10^{-3} M) in the presence of $HClO_4$ (2.5×10^{-3} M) in deaerated C_2H_5CN at 203 K under photoirradiation with a high-pressure Hg lamp (1000 W). The asterisks denote an Mn marker. (b) The simulated spectrum with ΔH_{msl} (maximum slope line width) = 1.8 G. (c) Hyperfine coupling constants obtained by DFT calculations. (d) The hyperfine coupling constants used for the simulation.

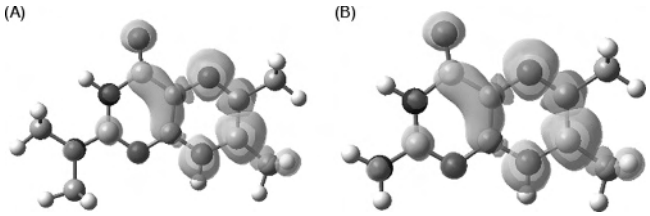

Figure 9. Spin distributions of monohydropterin radicals for $H_2dmdmp^{\bullet}$ (A) and $H_2dmp^{\bullet}$ (B). Protons are located at the N3 and N8 positions.

The calculated atomic spin densities at N5, C6, C7, and N8 for $H_2dmdmp^{\bullet}$ and $H_2dmp^{\bullet}$ were 0.432, 0.134, 0.379, and 0.174 and 0.434, 0.136, 0.382, and 0.173, respectively. The order of the spin densities is N5 > C7 > N8 ≈ C6.

Formation of $H_4dmp^{+\bullet}$ as a transient species has been reported by Yamauchi and co-workers in the course of the oxidation of the fully reduced form (H_4dmp) by Cu(II) ion.[45] They observed an ESR signal exhibiting hyperfine coupling constants that indicate that the unpaired electron also delocalizes on the PCET region (N5−C6−C7−N8) as observed for the radicals described in this paper. In their case, the pterin cation radical was not bound to the Cu ion; therefore, the radical was postulated to undergo rapid disproportionation to form a mixture of nonradical species, H_2dmp and H_4dmp. On the contrary, our Ru−pterin complexes are stable enough to exhibit reversible PCET, and those radical intermediates are stabilized in their coordination spheres due to not only coordination to the positively charged metal center but also strong π-back-bonding interactions to prevent them from their disproportionation. Thus, a diamagnetic and cationic Ru^{II}−TPA coordination environment is suitable for investigation of radical intermediates derived from redox reactions of heteroaromatic coenzymes and their electronic structures using ESR spectroscopy.

(45) Funahashi, Y.; Kohzuma, T.; Odani, A.; Yamauchi, O. *Chem. Lett.* **1994**, 385−388.

Summary

We described the synthesis and characterization of Ru(II)−pterin complexes exhibiting clear reversible PCET including formation of stable radical intermediates. The Ru(II) center is important to hold the protonated and positively charged pterin ligands in the coordination spheres by a π-back-bonding interaction with the protonated pterins. The doubly protonated complexes of **1** and **3** exhibited clear and reversible reduction processes to generate the ruthenium-bound monohydropterin radicals upon one-electron reduction using both electrochemical reduction and photoinduced electron-transfer reduction. Those radicals can be stabilized by coordinating to the Ru−TPA units to allow us to observe their ESR signals to elucidate their electronic structures in which the unpaired electron delocalizes in the PCET region of the pyrazine moiety of the pterin skeleton.

Substitution of the amino group at the 2-position in the pterin structure to the *N*,*N*-dimethylamino group has no significant impact to the redox potentials and pK_a values. However, the 2-amino group is important to stabilize a quinonoid form among the resonance structures as depicted in Scheme 4 by virtue of intermolecular hydrogen bonding as evidenced by the crystal structure of **3**. The crystal structure also indicates the high proton accessibility at the N-8 position in the PCET, probably due to the contribution of the quinonoind form.

Acknowledgment. We are grateful to Dr. Yasuhiro Funahashi (Nagoya Institute of Technology, Japan) for his invaluable guidance in preparing Hdmdmp. We thank Dr. Mikio Yasutake (Kyushu University, Fukuoka, Japan) for his expertise in X-ray crystallography on **1**. We also appreciate Prof. James M. Mayer (University of Washington, Seattle) for his helpful discussion and suggestion. This work has been supported by Grants-in-Aid (No. 16550057 to T. K.).

Supporting Information Available: Crystallographic data (CIF format), a description of the hydrogen-bonding networks in the crystal of **3**, spectroscopic titration for **3**, and a lift of hyperfine coupling constants calculated by various basis data sets in DFT calculations. This material is available free of charge via the Internet at http://pubs.acs.org.

IC701759C